# Steering the Electron in $H_2^+$ by Nuclear Wave Packet Dynamics

Bettina Fischer,[1] Manuel Kremer,[1] Thomas Pfeifer,[1] Bernold Feuerstein,[1] Vandana Sharma,[1] Uwe Thumm,[2]
Claus Dieter Schröter,[1] Robert Moshammer,[1] and Joachim Ullrich[1]

[1]*Max-Planck-Institut für Kernphysik, Saupfercheckweg 1, D-69117 Heidelberg, Germany*
[2]*James R. Macdonald Laboratory, Kansas State University, Manhattan, Kansas 66506-2606, USA*
(Received 2 July 2010; revised manuscript received 8 September 2010; published 22 November 2010)

By combining carrier-envelope phase (CEP) stable light fields and the traditional method of optical pump-probe spectroscopy we study electron localization in dissociating $H_2^+$ molecular ions. Localization and localizability of electrons is observed to strongly depend on the time delay between the two CEP-stable laser pulses with a characteristic periodicity corresponding to the oscillating molecular wave packet. Variation of the pump-probe delay time allows us to uncover the underlying physical mechanism for electron localization, which are two distinct sets of interfering dissociation channels that exhibit specific temporal signatures in their asymmetry response.

The availability of intense femtosecond laser pulses has led to remarkable achievements in the field of atomic and molecular physics over the last few years. These ultrashort laser pulses represent a powerful tool to manipulate the making and breaking of molecular bonds with the perspective to control chemical reactions (see, e.g., [1,2]). With ever shorter pulses containing only a few optical cycles, the carrier-envelope phase (CEP), i.e., the relative phase between the pulse envelope and the electric field of the carrier wave, has become an important parameter as it determines the exact shape of the laser field on a subfemtosecond time scale. Recent experiments [3,4] showed that the CEP can be used to control the emission direction of $H^+$ or $D^+$ fragments in dissociating hydrogen or deuterium molecular ions, thus demonstrating electron localization in a laser-induced, simple chemical reaction. The physical mechanism responsible for the CEP-dependent "left-right" asymmetry of electron localization in dissociating molecules was thus far broadly interpreted as quantum interference among at least two electronic states in molecules: The ionization of hydrogen or deuterium by an ultrashort laser pulse leads to the creation of a coherent nuclear wave packet (NWP) in the electronic ground ($1s\sigma_g$) [4] or excited state ($2p\sigma_u$) [3] of the molecular ion. The NWP then moves towards larger internuclear distances where the energy gap between the $1s\sigma_g$ and the $2p\sigma_u$ state becomes smaller, such that the laser can resonantly couple the two states and population is transferred between them. The coherent superposition of the gerade and the ungerade state finally leads to a localization of the electron at either the left or the right nucleus with a preference that is controlled by the CEP. An alternative approach to induce electron localization was recently demonstrated by using the time delay between an attosecond pulse [5] or pulse train [6] and an IR probe pulse as control parameter.

However, the experiments conducted so far did not analyze the dependence of electron localization on the shape and dynamics of the NWP. While some of the experimental results [4] appear to be in good agreement with theoretical predictions [7,8] that ignore the dynamical behavior of the NWP after the first ionization step by using an incoherent average of populated vibrational states, a very recent simulation [9] shows that the evolution of the molecular wave packet after ionization (and thus the coherence among the vibrational states) leads to a time-delay-dependent asymmetry that was not considered in earlier theoretical models. In fact, experimental [10,11] as well as theoretical [12–14] investigations revealed that the shape of the NWP in $H_2^+$ ($D_2^+$), evolving freely after strong-field ionization by a pump pulse, undergoes significant changes with increasing time up to a complete dephasing, where the wave function is delocalized over the whole potential well, followed by several revivals [12,15], where the NWP is localized and oscillates.

In this Letter we experimentally combine the pump-probe approach with CEP-control technology to specifically target the electronic quantum interference process that leads to electron localization in dissociating $H_2^+$. By using linearly polarized CEP-stable pump and probe pulses and choosing a time-delay in the wave packet revival region we were able to study the quantum interference process isolated from the ionization process. The first (pump) pulse ionizes an $H_2$ molecule and creates a NWP. The second (probe) pulse, which arrives after a well-defined time delay, induces the dissociation of $H_2^+$ by coupling the $1s\sigma_g$ and $2p\sigma_u$ states, leading to electron localization. By changing the time delay between the two pulses, the influence of the NWP dynamics on the left-right asymmetry is studied. We demonstrate that in the revival region both the CEP and the pump-probe delay time serve as efficient control parameters. This combination of pump-probe and CEP control allows us to extract the physical mechanism underlying electron localization. We find two qualitatively different interference mechanisms at work at

the same time: One that is governed by coherence among vibrational states and another one that is largely insensitive to the pump-probe delay and thus independent of vibrational coherence.

In the experiment we used ultrashort (6 fs, 760 nm) laser pulses with stabilized CEP. A glass wedge was moved in and out of the laser beam for continuous CEP sweeping before the beam was fed through a Mach-Zehnder type interferometer with one arm variable in length, providing two pulses with a fixed relative CEP separated by a time delay which can be scanned (0.3 fs resolution). The laser pulses (approximately equal intensities of 0.4 PW/cm$^2$) were focused onto a supersonic jet of $H_2$ in the ultrahigh vacuum chamber ($10^{-11}$ mbar) of a reaction microscope [16]. The protons emerging from dissociation of $H_2^+$ were guided by weak electric fields (2 V/cm) onto a position-sensitive channel-plate detector. By measuring the times of flight and the positions where the ions hit the detector, their three-dimensional momentum vectors can be reconstructed.

To exclude events for which the dissociation was already induced by the pump pulse, the polarization axes of the two laser pulses were chosen at 90° relative to each other. The ionization probability of $H_2$ is almost orientation independent [17,18], whereas the coupling between the gerade and the ungerade state is most efficient when the $H_2^+$ molecular axis is aligned along the laser polarization axis. The experimental data shown below include only those events, where the proton was emitted into an angular cone of ±30° with respect to the polarization axis of the probe pulse effectively selecting situations in which the pump pulse prepares the NWP in $H_2^+$ that is used as a well-defined, coherent initial quantum state for the probe pulse. Note, we cannot discriminate against cases for which both steps, ionization and dissociation, occurred in the probe pulse resulting in a delay-independent background.

To characterize the electron localization, the experimentally accessible asymmetry parameter $A = (N_L - N_R)/(N_L + N_R)$ is calculated as the normalized difference of the number of events for which the proton was emitted into the left ($N_L$) vs the right ($N_R$) hemisphere with respect to the probe-pulse polarization axis.

Analysis of the experimental data (Fig. 1) reveals a correlation between NWP dynamics and electron localization. In Fig. 1(a) the proton yield integrated over all CEP values is shown in dependence of the kinetic energy release (KER) and the pulse delay. It reveals a periodicity of about 18 fs emerging from the NWP oscillation in the $1s\sigma_g$ potential well. The asymmetry parameter $A$ is shown in Figs. 1(b)–1(e) as a function of KER and CEP for different delay times as marked by the vertical lines in Fig. 1(a). A delay-dependent change of the asymmetry pattern is visible, which correlates with the time-dependent dissociation yield (18 fs periodicity). Consequently, Figs. 1(b) and 1(d) as well as 1(c) and 1(e) show a pairwise agreement appearing as
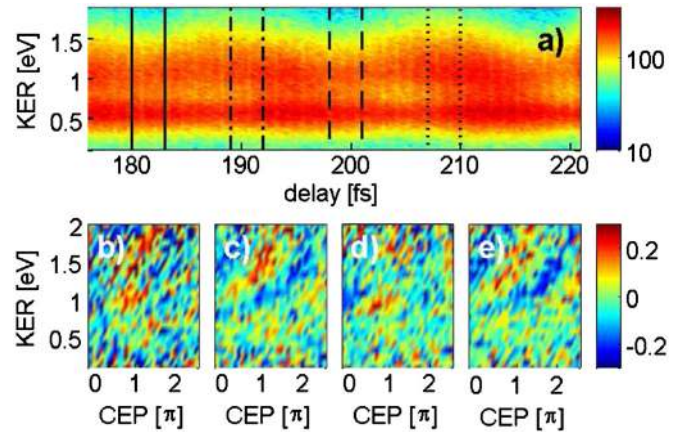


FIG. 1 (color online).   (a) Proton count rate after dissociation as a function of the kinetic energy release (KER) and the delay between pump and probe pulse integrated over all CEP values. (b)–(e) Measured proton asymmetry in dependence of the CEP and the KER for delays between (b) 178–181, (c) 189–192, (d) 198–201, and (e) 207–210 fs, as marked by the vertical lines in (a).

continuous stripes between 1–2 eV in Figs. 1(c) and 1(e) which are not visible in 1(b) and 1(d).

In order to obtain a deeper insight into the dependence of electron localization on the NWP dynamics, we analyze the asymmetry as a function of delay time. The CEP and delay-dependent asymmetry is shown for two different KER ranges in Figs. 2(a) and 2(b). For intermediate KER [Fig. 2(a)] the asymmetry reveals a strong delay dependence with pronounced maxima and minima, which repeat with the periodicity of the NWP oscillation. Thus, by keeping the value of the CEP fixed, the degree of electron
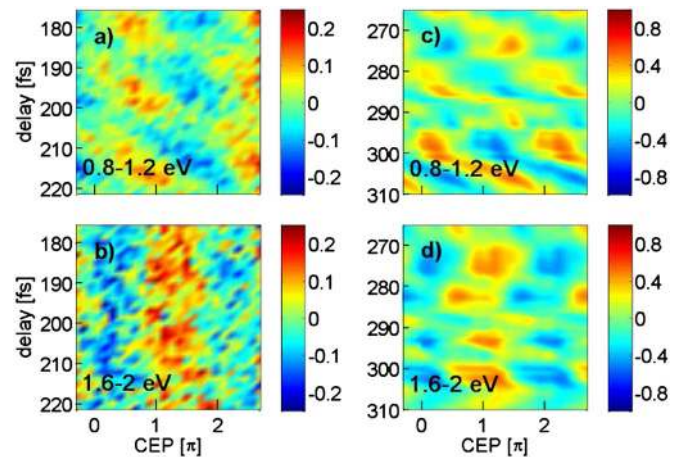


FIG. 2 (color online).   The measured asymmetry as a function of the delay and the carrier-envelope phase is shown for the wave packet revival region for (a) a KER between 0.8–1.2 eV and (b) a KER between 1.6–2 eV. The right-hand images represent the asymmetry obtained from the wave packet propagation calculations at corresponding delays for a KER between (c) 0.8–1.2 and (d) 1.6–2 eV (see text).

localization can be steered solely by the delay. Furthermore, the regions of maximum asymmetry form "tilted stripes", i.e., the asymmetry pattern shifts relative to the CEP axis with the same periodicity as the NWP. By contrast, for higher KER [Fig. 2(b)] the asymmetry pattern is (within statistical fluctuations) rather independent of the delay on a large scale of 10 fs or more. These results indicate that different physical mechanisms lead to electron localization for the two KER ranges.

Before discussing the underlying physics and to validate our experimental results, we compare our data with results obtained from wave packet propagation calculations considering exclusively the two lowest-lying electronic states in $H_2^+$. To this end, the one-dimensional time-dependent Schrödinger equation was solved by using a Crank-Nicholson split-operator method [15,19]. The electric field of the first pulse was not explicitly considered as due to the perpendicular polarization of the two pulses in the experiment, it cannot induce any asymmetry. A more detailed description of the calculation procedure can be found in [4].

The results of the calculation for a 6 fs probe pulse with an intensity of 0.4 PW/cm² are shown in Figs. 2(c) and 2(d). Note that the delay range in the calculations does not coincide with the one of the measurements. Earlier investigations [20,21] showed that a pulse pedestal and/or satellite pulses shift the revival towards shorter delay times. The delay ranges in this Letter are chosen such that for calculated and measured results the same relative delay with respect to the revival is considered. In agreement with the experimental findings, the regions of maximal asymmetry form tilted stripes for intermediate KER, whereas for high KER the asymmetry maxima line up vertically around a CEP of about $1\pi$ for all delays. This qualitative agreement justifies the assumption that only the two lowest states in $H_2^+$ contribute significantly. Together with the experimental results, these findings suggest two qualitatively different interference mechanisms that occur in different KER ranges and will now be discussed.

A prerequisite for electron localization in an inversion-symmetric system such as $H_2^+$ is the coherent superposition of states with different parities. In the experimentally observed asymptotic limit ($R \rightarrow \infty$) this can only occur when different (above-threshold) dissociation (ATD) paths [22] lead to the same KER and thus interfere [8]. The relevant channels are shown in Fig. 3. For the intensities used in our experiment the dissociation occurs mainly via the $1\omega$ and $2\omega$ channels ($\omega$: laser frequency). As illustrated in Fig. 3 the $1\omega$ process occurs at large $R$ where the photon energy matches the energy difference between the $1s\sigma_g$ and the $2p\sigma_u$ potential curves. By contrast, the $2\omega$ channel requires the absorption of three photons (due to parity) followed by emission of one photon resulting in a net absorption of two photons and in higher KERs. In the experiment these $1\omega$ and $2\omega$ channels and a weak
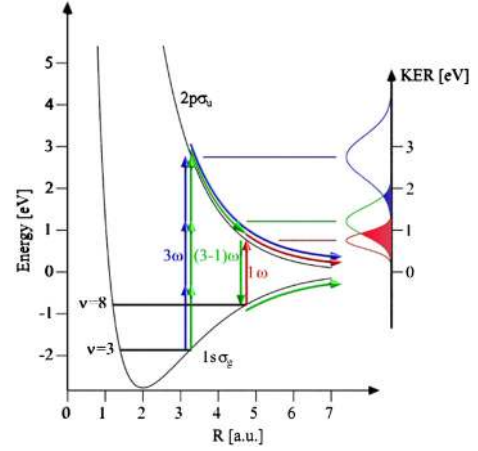


FIG. 3 (color online). (a) Illustration of the dissociation via absorption of three photons ($3\omega$, blue arrows), net-absorption of two photons [$(3 - 1)\omega = 2\omega$, green arrows], and via absorption of one photon ($1\omega$, red arrow). On the right side the corresponding KER distributions are plotted. Interference and thus asymmetry can occur where the different paths overlap in energy (blue and red shaded areas).

contribution from the $3\omega$ channel are visible. The two lowest channels appear in Fig. 1(a) as two KER bands centered around 0.6 eV ($1\omega$) and 1.2 eV ($2\omega$), respectively. Because of the large laser bandwidth, the KER distributions for the different channels partially overlap as indicated by the red and blue shaded areas in Fig. 3, so that interference between these channels occurs.

Regarding the KER ranges where the distributions overlap, we interpret our measured asymmetry as being due to interference between the $1\omega$ and $2\omega$ channels (intermediate KER) and between the $2\omega$ and $3\omega$ channels (high KER), respectively.

The bound wave packet motion determines mainly the relative population of the $1s\sigma_g$ and $2p\sigma_u$ electronic states and thus the contrast of the asymmetry. The phase shift of the asymmetry in the $2\pi$-periodic CEP dependence, however, depends on the relative phase $\Delta\phi_{g,u} = \phi_g - \phi_u$ between the outgoing dissociative wave packets of gerade ($g$) or ungerade ($u$) parity. For a given KER, $\phi_{g,u}$ has effectively two contributions: $\phi_{g,u} = \phi_i(\tau) + \phi_{ATD}^{n\omega}(CEP, KER)$. Here, $\phi_i(\tau)$ comes from the initial bound wave packet and depends on the delay $\tau$ and $\phi_{ATD}^{n\omega}(CEP, KER)$ is the CEP-dependent phase arising from the transition from the initial state to the $n$-photon ATD channel which also contains the semiclassical phase of the wave packet on the way out. Since the initial wave packet is a superposition of vibrational eigenstates, $\phi_{ATD}^{n\omega}(CEP, KER)$ will be delay-independent for each single eigenstate $v$ since only a non-observable global phase is changing. In addition, the ATD transitions address not all eigenstates uniformly but rather define two Franck-Condon absorption windows around $v = 3$ and $v = 8$, where $1\omega$ and $3\omega$ transitions become resonant. For the three channels shown in Fig. 3 we find
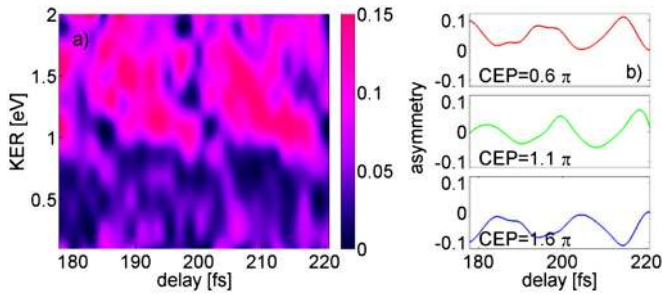
FIG. 4 (color online). (a) Amplitude (absolute value) of the asymmetry (electron localizability) measured in the revival region as a function of the delay and the KER. (b) Delay-dependent asymmetry for three different CEP values obtained for a KER between 0.8 and 1.2 eV. The amplitude was obtained by fitting a sinusoidal function along the CEP axis for KER ranges of 0.2 eV to smoothen statistical fluctuations.

$$\phi_u^{1\omega} = \phi_i^{v\approx 8}(\tau) + \phi_{\mathrm{ATD}}^{1\omega}(\mathrm{CEP}, \mathrm{KER}),$$
$$\phi_g^{2\omega} = \phi_i^{v\approx 3}(\tau) + \phi_{\mathrm{ATD}}^{2\omega}(\mathrm{CEP}, \mathrm{KER}),$$
$$\phi_u^{3\omega} = \phi_i^{v\approx 3}(\tau) + \phi_{\mathrm{ATD}}^{3\omega}(\mathrm{CEP}, \mathrm{KER}).$$

The interference of the $2\omega$ and $3\omega$ channels starts from the same band of vibrational states around $v = 3$ and thus the delay-dependent phase of the initial states drops out of the relative phase $\Delta\phi_{g,u}$, leading to the near-vertical (delay-independent) alignment of the asymmetry maxima at high KER observed in the experiment and the simulation. On the other hand, interference of the $1\omega$ and $2\omega$ channels at lower KER involves two different vibrational bands which leads to a delay dependence of the relative phase $\Delta\phi_{g,u}$ and thus a delay-dependent CEP value of the position of the maximum asymmetry (tilted stripes).

As mentioned above, the wave packet motion modulates also the relative populations of the $1s\sigma_g$ and the $2p\sigma_u$ states and thus determines the maximum strength of the asymmetry which can be obtained for a certain delay and KER value by varying the CEP. This is further analyzed in Fig. 4(a), where we show the amplitude of the CEP-dependent asymmetry variation plotted vs KER and time delay. It reveals a pronounced delay dependence, in particular, for the interference between the $1\omega$ and the $2\omega$ dissociation channels at intermediate KERs, showing that the degree of CEP-dependent electron localization, i.e., the *localizability* of the electron can be controlled by the delay. The origin of this control is that an efficient laser-induced population transfer between the $1s\sigma_g$ and the $2p\sigma_u$ state only occurs when the oscillating NWP passes the regions where the $1\omega$ or $3\omega$ transitions are resonant. The amplitude and sign of the asymmetry thus depends on both, the delay and the CEP. This is illustrated in Fig. 4(b), where the asymmetry is shown for three different CEP values at a KER between 0.8 eV and 1.2 eV as a function of the delay. For given CEPs the asymmetry can be changed just by changing the delay, i.e., the NWP dynamics fully controls

at which nucleus the electron remains predominantly localized.

In conclusion, we extracted and analyzed the different physical mechanisms responsible for electron localization in $H_2^+$ after strong-field ionization. This was made possible by using a CEP-pump-probe scheme, allowing us to separate the ionization from the dissociation step. By analyzing the temporal signature of the asymmetry, two different interference mechanism were identified: At lower KER a clear delay-dependent shift of the asymmetry was observed, whereas the asymmetry at higher KER appears to be almost delay-independent. This was explained by the interference between multiple above-threshold dissociation channels involving a different number of effectively absorbed photons, but initiating from either the same (higher KER) or different (lower KER) coherently populated vibrational states. Electron localization and localizability after strong-field ionization was thus found to depend on vibrational coherence to an extent governed by the specific pairwise interfering dissociation pathways. The closer understanding of the physics underlying the manipulation of a bound electron obtained by investigating dissociating $H_2^+$ will help in the future to reach a stronger level of control over more complex molecules and thus represents a qualitiative step forward in controlling chemical reactions on an electronic level.

[1] T. Brixner, Chem. Phys. Chem. **4**, 418 (2003).
[2] M. Wollenhaupt, J. Phys. Phys.: Conf. Series **88**, 012053 (2007).
[3] M. F. Kling et al., Science **312**, 246 (2006).
[4] M. Kremer et al., Phys. Rev. Lett. **103**, 213003 (2009).
[5] G. Sansone et al., Nature (London) **465**, 763 (2010).
[6] K. P. Singh et al., Phys. Rev. Lett. **104**, 023001 (2010).
[7] V. Roudnev and B. D. Esry, Phys. Rev. A **76**, 023403 (2007).
[8] J. J. Hua and B. D. Esry, J. Phys. B **42**, 085601 (2009).
[9] C. R. Calvert et al., J. Phys. B **43**, 011001 (2010).
[10] Th. Ergler et al., Phys. Rev. Lett. **97**, 193001 (2006).
[11] L. B. Madsen, Phys. Rev. A **65**, 053417 (2002).
[12] B. Feuerstein and U. Thumm, Phys. Rev. A **67**, 063408 (2003).
[13] J. H. Posthumus, Rep. Prog. Phys. **67**, 623 (2004).
[14] A. D. Bandrauk, S. Chelkowski, and H. S. Nguyen, Int. J. Quantum Chem. **100**, 834 (2004).
[15] B. Feuerstein et al., Phys. Rev. Lett. **99**, 153002 (2007).
[16] V. L. B. de Jesus et al., J. Electron Spectrosc. Relat. Phenom. **141**, 127 (2004).
[17] M. Magrakvelidze et al., Phys. Rev. A **79**, 033408 (2009).
[18] I. V. Litvinyuk et al., Phys. Rev. Lett. **90**, 233003 (2003).
[19] U. Thumm et al., Phys. Rev. A **77**, 063401 (2008).
[20] A. Rudenko et al., Chem. Phys. **329**, 193 (2006).
[21] T. Niederhausen, Ph.D. thesis, Kansas State University, Manhattan KS, USA, 2007.
[22] A. Giusti-Suzor et al., J. Phys. B **28**, 309 (1995).